Inorganic Chemistry

Article

pubs.acs.org/IC

Structural Diversity and Physical Properties of Paramagnetic Molecular Conductors Based on Bis(ethylenedithio)tetrathiafulvalene (BEDT-TTF) and the Tris(chloranilato)ferrate(III) Complex

Matteo Atzori,[†,‡] Flavia Pop,[‡] Pascale Auban-Senzier,[§] Carlos J. Gómez-García,[⊥] Enric Canadell,[¶] Flavia Artizzu,[†] Angela Serpe,[†] Paola Deplano,[†] Narcis Avarvari,*[,‡] and Maria Laura Mercuri*[,†]

[†]Dipartimento di Scienze Chimiche e Geologiche, Università degli Studi di Cagliari, S.S. 554 − Bivio per Sestu − I09042 Monserrato, Cagliari, Italy

[‡]Laboratoire MOLTECH-Anjou UMR 6200, UFR Sciences, CNRS, Université d'Angers, Bât. K, 2 Bd. Lavoisier, 49045 Angers, France

[§]Laboratoire de Physique des Solides, UMR 8502, Université Paris-Sud, Bât. 510, 91405 Orsay, France

[⊥] Instituto de Ciencia Molecular (ICMol), Parque Científico, Universidad de Valencia, C/Catedrático José Beltrán, 2, 46980 Paterna, Spain

[¶]Institut de Ciència de Materials de Barcelona (CSIC), Campus de la UAB, E-08193 Bellaterra, Spain

Supporting Information

ABSTRACT: Electrocrystallization of bis(ethylenedithio)tetrathiafulvalene (BEDT-TTF) in the presence of the tris(chloranilato)ferrate(III) $[Fe(Cl_2An)_3]^{3-}$ paramagnetic chiral anion in different stoichiometric ratios and solvent mixtures afforded three different hybrid systems formulated as $[BEDT\text{-}TTF]_3[Fe(Cl_2An)_3]\cdot 3CH_2Cl_2\cdot H_2O$ (**1**), δ-$[BEDT\text{-}TTF]_5[Fe(Cl_2An)_3]\cdot 4H_2O$ (**2**), and α'''-$[BEDT\text{-}TTF]_{18}[Fe(Cl_2An)_3]_3\cdot 3CH_2Cl_2\cdot 6H_2O$ (**3**). Compound **1** presents an unusual structure without the typical alternating organic and inorganic layers, whereas compounds **2** and **3** show a segregated organic−inorganic crystal structure where layers formed by Λ and Δ enantiomers of the paramagnetic complex, together with dicationic BEDT-TTF dimers, alternate with layers where the donor molecules are arranged in the δ (**2**) and α''' (**3**) packing motifs. Compound **1** behaves as a semiconductor with a much lower conductivity due to the not-layered structure and strong dimerization between the fully oxidized donors, whereas **2** and **3** show semiconducting behaviors with high room-temperature conductivities of ca. 2 S cm^{-1} and 8 S cm^{-1}, respectively. The magnetic properties are dominated by the paramagnetic $S = 5/2$ $[Fe(Cl_2An)_3]^{3-}$ anions whose high-spin character is confirmed by electron paramagnetic resonance and magnetic susceptibility measurements. The correlation between crystal structure and conductivity behavior was studied by means of tight-binding band structure calculations, which support the observed conducting properties.

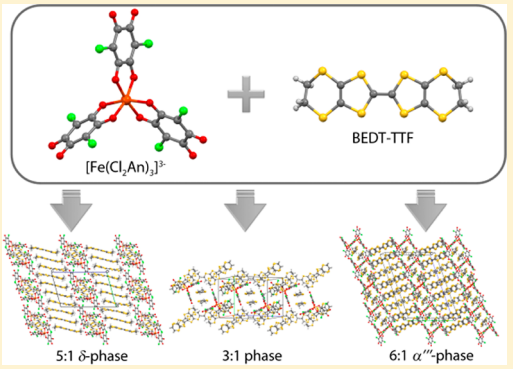

INTRODUCTION

Molecular materials combining conducting (delocalized π electrons) and magnetic (localized d electrons) properties have attracted major interest in molecular science since they can exhibit coexistence of two distinct physical properties, furnished by the two networks, or novel and improved properties due to the interactions established between them.[1−3] The development of these π−d systems as multifunctional materials represents one of the main targets in current materials science for their potential applications in molecular electronics.[1] Important milestones in the field of magnetic molecular conductors have been achieved using as molecular building blocks the bis(ethylenedithio)-tetrathiafulvalene (BEDT-TTF) organic donor[2] or its selenium derivatives and charge-compensating anions ranging from simple mononuclear complexes $[MX_4]^{n-}$ (M = Fe^{III}, Cu^{II}; X = Cl, Br)[3a,b,e] and $[M(ox)_3]^{3-}$ (ox = oxalate = $C_2O_4^{2-}$)[1a,2,4] with tetrahedral and octahedral geometries to layered structures such as the bimetallic oxalate-based layers of the type $[M^{II}M^{III}(ox)_3]^-$ (M^{II} = Mn, Co, Ni, Fe, Cu; M^{III} = Fe, Cr).[5] In these systems the shape of the anion and the arrangement of intermolecular contacts, especially hydrogen-bonding, between the anionic and cationic layers influence the packing motif of the BEDT-TTF radical cations and therefore the physical properties of the charge-transfer salt.[6] Tris-chelated metal complexes with octahedral geometry are among the most successful counterions for favoring enhanced intermolecular

Received: April 29, 2014
Published: June 13, 2014

   dx.doi.org/10.1021/ic501001r | Inorg. Chem. 2014, 53, 7028−7039

interactions between donors and hence good transport properties, thanks to their capability to provide organic−inorganic segregation, compared to square-planar complexes, such as d^8 metal dithiolenes, which favor instead mixed organic−inorganic stacks and thus semiconducting or insulating states. In addition, they have the possibility of a specific assembly order of Λ and Δ chirality that may influence the packing and thus the physical properties of the material as well as to introduce functionalities such as magnetic properties through both the metal and a suitably tailored ligand. Typically, the structure of these materials is formed by segregated stacks of the organic donors and the inorganic counterions which add the second functionality to the conducting material. The intermolecular interactions, in particular van der Waals interactions (S···S, Se···Se, shorter than the sum of the van der Waals radii), $\pi-\pi$, halogen-bonding, H-bonding, etc., play a crucial role in self-assembling these predesigned molecular units and may provide a powerful way to afford layered multifunctional molecular materials with new or unknown physical properties. The first paramagnetic superconductor [BEDT-TTF]$_4$[$(H_3O)Fe^{III}(ox)_3$]·C_6H_5CN[2a] and the first ferromagnetic conductor [BEDT-TTF]$_3$[$Mn^{II}Cr^{III}(ox)_3$][5c] were successfully obtained by electrocrystallizing the mononuclear $[Fe(ox)_3]^{3-}$ and the $[Mn^{II}Cr^{III}(ox)_3]^-$ (two-dimensional (2D) honeycomb with oxalate bridges) anions with the BEDT-TTF organic donor, as magnetic and conducting carriers, respectively. Furthermore, by combining the bis(ethylenedithio)-tetraselenafulvalene (BETS) molecule with the zero-dimensional $FeCl_4^-$ anion, a field-induced superconductivity with $\pi-d$ interaction was observed, which may be mediated through S···Cl interactions between the BETS molecule and the anion.[3a] Clues for designing the molecular packing in the organic network, which sustains the conducting properties, were provided by the use of the paramagnetic chiral anion $[Fe(croc)_3]^{3-}$ (croc = croconate = $C_5O_5^{2-}$) as magnetic component of two dual-function materials. This chiral anion led to the synthesis of two systems: α-[BEDT-TTF]$_5$[$Fe(croc)_3$]·$5H_2O$, which behaves as a semiconductor with a high room-temperature conductivity (ca. 6 S cm^{-1}) and β-[BEDT-TTF]$_5$[$Fe(croc)_3$]·C_6H_5CN, which shows a high room-temperature conductivity (ca. 10 S cm^{-1}) and a metallic behavior to ca. 140 K.[7] The BEDT-TTF molecules in the α-phase are arranged in a herringbone packing motif, which is induced by the chirality of the anions. The alternation of Δ and Λ enantiomers along the *b* axis is the driving force that induces the same alternation of "right" and "left" turned columns along this direction, representing, as far as we know, the first example of chirality-induced α-phase. This effect is likely due to the presence of a supramolecular interlayer S···O cation−anion interaction (3.01 Å), shorter than the sum of the corresponding van der Waals radii (3.32 Å), together with steric effects. Therefore, the packing of the organic network and the corresponding conducting properties can be influenced by playing with the size, shape, symmetry, and charge of the inorganic counterions. In this respect, anilato-based metal complexes[8] are very interesting molecular building blocks to be used as paramagnetic counterions, also because they offer the opportunity of exchange coupling at great distance through the anilate bridge, being therefore extremely versatile in the construction of the above-mentioned conducting/magnetic and magnetic molecule-based materials. Very recently, the new family of paramagnetic tris(haloanilato)metalate(III) complexes, $[M^{III}(X_2An)_3]^{3-}$ (M = Fe, Cr; X = Cl, Br, I, An = anilate = $C_6O_4^{2-}$), based on the 3,6-dihalo derivatives of 2,5-dihydroxybenzoquinone ($H_4C_6O_4$), chloranilate (Cl_2An^{2-}), bromanilate (Br_2An^{2-}), and iodanilate (I_2An^{2-}), has been described by some of us,[9] with the aim of investigating the role of the halogen substituents on the physical properties of the materials which stem from self-assembling these molecular building blocks. In particular, the Cr(III) complexes have been successfully used for the preparation of a new family of layered chiral porous molecular magnets with tunable ordering temperatures, formulated as $A[Mn^{II}Cr^{III}(X_2An)_3]\cdot G$ (A = $[(H_3O)(phenazine)_3]^+$ and NBu_4^+; X = Cl, Br, I and H; G = CH_3COCH_3 and H_2O).[10] With the aim of studying new multifunctional materials whose physical properties may be tuned by changes on the molecular structures of their building units, we combine here the tris(chloranilato)ferrate(III) $[Fe(Cl_2An)_3]^{3-}$ complex anion as paramagnetic building block, with the BEDT-TTF organic donor as a potential building block of conducting layers. By varying the stoichiometric ratio of the components and the solvent mixture, three different hybrid systems formulated as [BEDT-TTF]$_3$[$Fe(Cl_2An)_3$]·$3CH_2Cl_2$·H_2O (**1**), δ-[BEDT-TTF]$_5$[$Fe(Cl_2An)_3$]·$4H_2O$ (**2**), and α‴-[BEDT-TTF]$_{18}$[$Fe(Cl_2An)_3$]$_3$·$3CH_2Cl_2$·$6H_2O$ (**3**) were obtained as some of the first examples of radical cation salts with the tris(chloranilato)ferrate(III) metal complex as counterion. We describe herein the synthesis, crystal structures, physical properties, and tight-binding band structure calculations of compounds **1**−**3** to study the correlation between crystal structure and conducting behavior.

RESULTS AND DISCUSSION

Synthesis. The tris(chloranilato)ferrate(III) complex $[PPh_4]_3[Fe(Cl_2An)_3]$[9] and the BEDT-TTF donor were combined in electrocrystallization experiments, using the same current density but different reagents stoichiometric ratios, and solvent mixture. Three different hybrid systems formulated as [BEDT-TTF]$_3$[$Fe(Cl_2An)_3$]·$3CH_2Cl_2$·H_2O (**1**), δ-[BEDT-TTF]$_5$[$Fe(Cl_2An)_3$]·$4H_2O$ (**2**), and α‴-[BEDT-TTF]$_{18}$[$Fe(Cl_2An)_3$]$_3$·$3CH_2Cl_2$·$6H_2O$ (**3**) were obtained as reported in Scheme 1. These systems mainly differ in the donor/anion ratio: 3:1, 5:1, and 6:1, for **1**, **2**, and **3**, respectively, which, along with the different crystallization

Scheme 1. Molecular Structures for the Complex Anion $[Fe(Cl_2An)_3]^{3-}$ (A) and the BEDT-TTF Organic Donor (D), and Experimental Condition Used for Obtaining Compounds 1−3

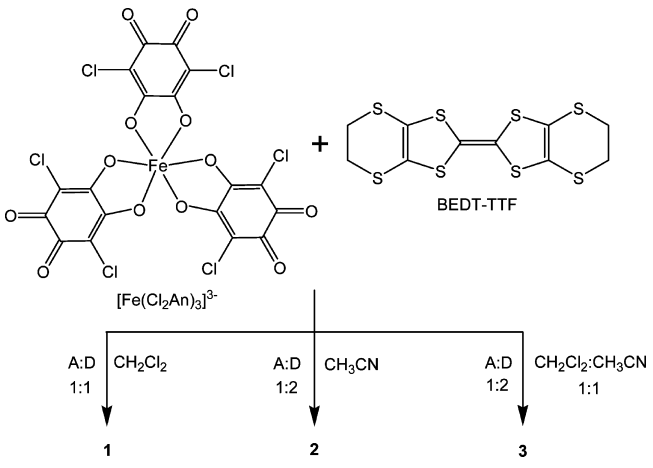

dx.doi.org/10.1021/ic501001r | Inorg. Chem. 2014, 53, 7028−7039

solvent molecules present in the structures, influences the crystal packing motif exhibited by the BEDT-TTF molecules in the organic layer and the resulting physical properties (*vide infra*).

Crystal Structures. The crystals structures of the three reported hybrid systems consist of homoleptic tris-chelated complex anions and BEDT-TTF radical cations. In each system, the metal complexes exhibit octahedral coordination geometry, with the iron(III) ion surrounded by six oxygen atoms of three chloranilate chelating ligands. These complexes are chiral according to the metal coordination, but both Λ and Δ enantiomers are present in the crystal lattices with intramolecular Fe···Fe distances of ca. 13.5 Å, which do not allow for a magnetic exchange interaction between metal centers (*vide infra*). In Figure 1 the molecular structure of the complex anion for **1** is reported.

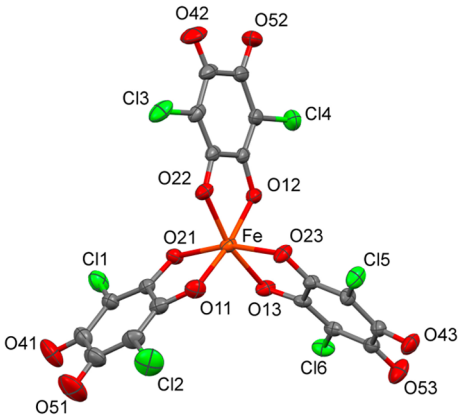

Figure 1. ORTEP drawing for the tris(chloranilato)ferrate(III) anionic complex (Δ enantiomer) for **1** with thermal ellipsoids at the 30% probability level.

The metal−oxygen bond distances in compounds **1**−**3** vary in the 1.994(7)−2.037(4) Å range and are very close to those observed for the $[PPh_4]^+$ salt of the same complex[9] (Table 1), suggesting the high spin character of the Fe(III) ions.

The C−O bond distances are influenced by the coordination to the metal center. The oxygen atoms coordinated to the metal have C−O distances on average 0.06 Å longer than those of the peripheral oxygen atoms, which show a major double bond character (Supporting Information, Table S1).

The X-ray analysis shows that **1** crystallizes in the triclinic centrosymmetric space group $P\bar{1}$ with three independent BEDT-TTF molecules (indicated as **A**, **B**, **C**) and one complex anion $[Fe(Cl_2An)_3]^{3-}$ in the asymmetric unit. The analysis of the bond distances for each crystallographically independent BEDT-TTF molecule, according to the procedure described by Day et al.,[11] reveals that each of the three donor molecules bear a charge of 1.0 ± 0.1, in agreement with the value of +3 expected for this salt (Table 2).

Table 2. Bond Distances Analysis and Selected Bond Distances (Å) for the BEDT-TTF Donor Molecules in 1

		A	B	C
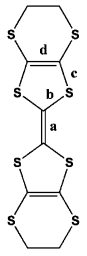	a	1.391(8)	1.388(8)	1.400(8)
	b	1.723(6)	1.716(6)	1.716(6)
		1.716(6)	1.725(6)	1.716(6)
		1.713(6)	1.716(6)	1.715(6)
		1.718(5)	1.719(6)	1.723(6)
	c	1.741(7)	1.744(6)	1.742(7)
		1.753(7)	1.735(6)	1.747(7)
		1.741(6)	1.747(7)	1.735(7)
		1.736(7)	1.744(7)	1.741(6)
	d	1.335(10)	1.338(10)	1.356(9)
		1.355(9)	1.342(8)	1.351(9)
δ = (b+c)-(a+d)	δ	0.724	0.734	0.704
Q = 6.347-7.4638·δ	Q	0.9(1)	0.9(1)	1.1(1)

The crystal packing of **1** is unusual and consists of two perpendicularly interpenetrated sublattices, one formed by dimers of **C** molecules separated by complex anions along the *ac* plane and the other formed by **B**−**A**−**A**−**B** tetramers of **A** and **B** molecules along the *bc* plane (Figure 2 and Supporting Information, Figure S1).

The role of the intermolecular interactions is crucial in determining the packing of the building blocks. Thus, in the **C**−**C** dimers, planar BEDT-TTF molecules are arranged in a face-to-face manner[12] forming isolated dimers that are surrounded by two metal complexes of opposite chirality establishing Cl···S interactions (Figure 3). This arrangement is similar to the one observed in the salt [BEDT-TTF]-[TRISPHAT]·CH_2Cl_2·CH_3CN[13] formed with the shape-related TRISPHAT anion $[P(C_6O_2Cl_4)_3]^-$, which presents the same tris-chelated chiral structure as $[Fe(Cl_2An)_3]^{3-}$ with tetrachlorinated phenyl rings.

The **A** and **B** molecules interact through S···S interactions forming dimers where the BEDT-TTF molecules are tilted 11° along the C═C double bond direction (torsion angle C5A−C6A−C6B−C5B). This molecular arrangement might be due to the lateral interactions between two **A** molecules of two consecutive **A**−**B** dimers, giving rise to a **B**−**A**−**A**−**B** tetramer (Figure 4).

The donor molecules arrangement in compound **1** (i.e., association in noninteracting dimers and tetramers), along with the fact that all the BEDT-TTF molecules bear a charge of +1, hinders a charge delocalization along the organic layers, in agreement with the semiconducting behavior and the low

Table 1. Fe−O Bond Distances (Å) for the Anionic Complex in Compounds 1−3 Compared with the Reported Values for $[PPh_4]_3[Fe(Cl_2An)_3]$[9]

bonds	1	2	3	$[PPh_4]_3[Fe(Cl_2An)_3]$
Fe−O(11)	1.996(5)	2.008(6)	2.020(6)	2.002(6)
Fe−O(21)	2.002(4)	2.022(6)	2.028(6)	2.008(6)
Fe−O(12)	2.018(4)	2.019(5)	1.994(7)	2.001(6)
Fe−O(22)	1.998(4)	1.999(6)	2.028(6)	2.017(6)
Fe−O(13)	2.026(4)	2.039(6)	2.018(6)	2.013(6)
Fe−O(23)	2.037(4)	2.014(6)	1.989(7)	1.999(6)
average Fe−O	2.013	2.017	2.013	2.007

dx.doi.org/10.1021/ic501001r | *Inorg. Chem.* 2014, 53, 7028−7039

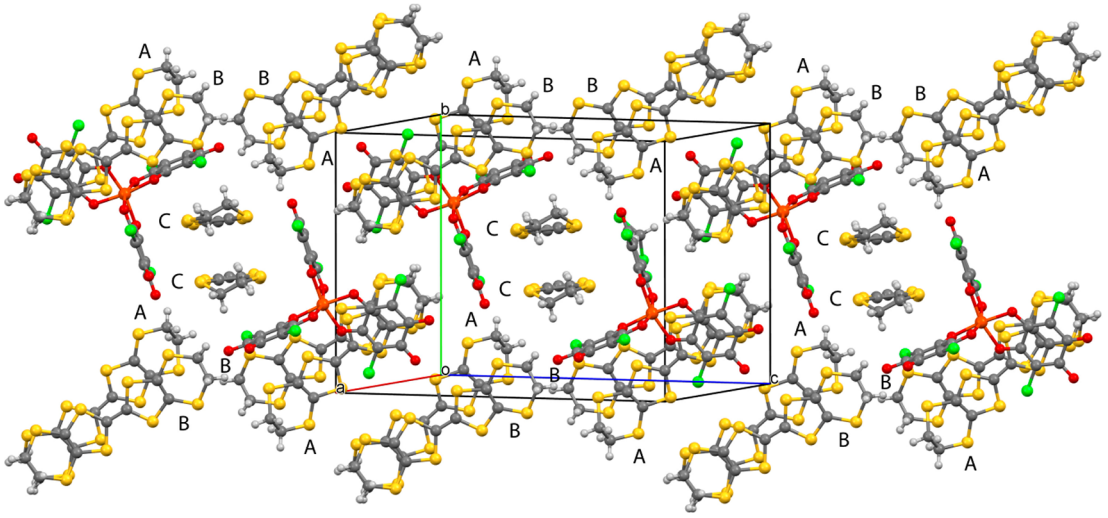

Figure 2. View of the crystal packing of **1** along the *bc* plane with labeled **A**, **B**, and **C** BEDT-TTF molecules. Crystallization water and CH_2Cl_2 molecules were omitted for clarity.

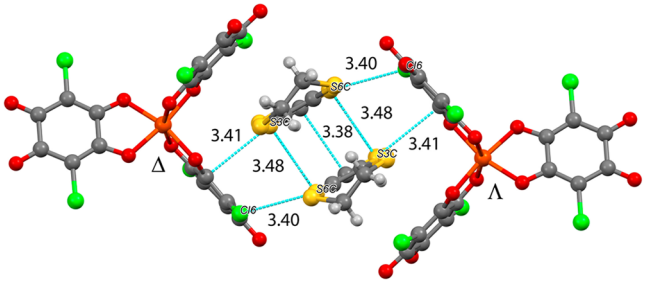

Figure 3. **C**−**C** dimer surrounded by two metal complexes of opposite chirality in **1**. Symmetry-related S···S contacts and intermolecular interactions lower than the sum of the van der Waals radii between the BEDT-TTF molecules and the chloranilate ligands are highlighted. (Å): S3C···S6C 3.48, S4C···S5C 3.57, Cl6···S6C 3.40, C13C···S6C 3.41.

conductivity at room temperature observed for this salt (*vide infra*).

Compound **2** crystallizes in the triclinic centrosymmetric space group $P\bar{1}$ with five independent BEDT-TTF molecules (indicated as **A**−**E**) and one complex anion $[Fe(Cl_2An)_3]^{3-}$ in the asymmetric unit. The crystal packing of **2** shows organic−inorganic layer segregation. The hybrid inorganic layer consists of BEDT-TTF dimers (**E**−**E**) surrounded by metal complexes as observed in compound **1** for the **C**−**C**-type dimer (*vide supra*). The purely organic layer is formed by the other four BEDT-TTF molecules (Figure 5).

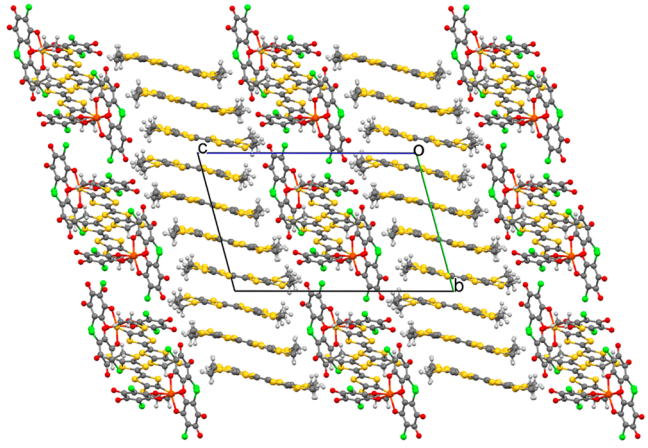

Figure 5. View of the crystal packing of **2** along the *bc* plane showing the organic−inorganic layer segregation. Crystallization water molecules were omitted for clarity.

The organic layer shows the **A**−**D** donor molecules arranged in the exotic δ-phase packing motif, which contains stacks of twisted BEDT-TTF dimer units.[12] The **A** and **C** molecules

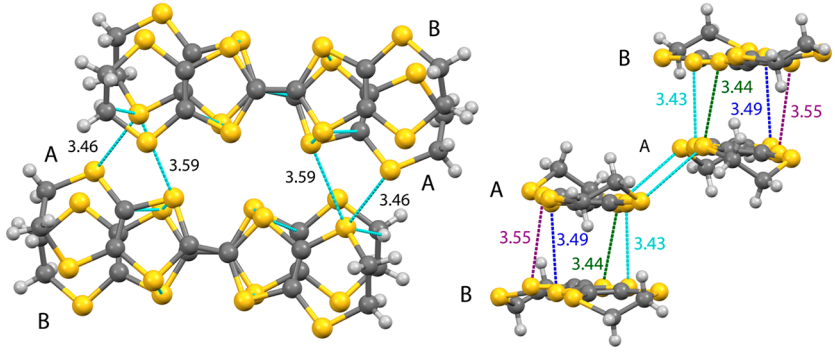

Figure 4. S···S contacts shorter than the sum of the van der Waals radii for the **B**−**A**−**A**−**B** tetramer in **1**. (Å): S1A···S7A 3.46, S3A···S7A 3.59, S3A···S3B 3.44, S4A···S4B 3.55, S5A···S5B 3.43, S6A···S6B 3.49.

dx.doi.org/10.1021/ic501001r | *Inorg. Chem.* 2014, 53, 7028−7039

interact laterally along *a*, showing alternated **A**−**A** and **C**−**C** dimer units, with S···S interdimer contacts (3.41−3.56 Å) shorter than the intradimer ones, that are longer than the sum of the van der Waals radii (3.65 Å). The **B** and **D** molecules are, instead, alternated in a **BD**−**DB** sequence (Figure 6). In this layer the shortest S···S contacts are found for the lateral interactions between the **B** and **D** molecules (3.43−3.46 Å). The oblique distances between the **D**−**D** molecules range from 3.57 to 3.60 Å, whereas those between the **B**−**B** molecules (3.62 Å) are longer. Between the two sublayers quite long S···S interactions are observed. These interactions are due to the typical twisted overlap mode of the δ phases, characterized, in the present case, by ω = 30.6° and D = 2.6 Å, where ω and D are the angle and the displacement between the molecular long axes, respectively.[12]

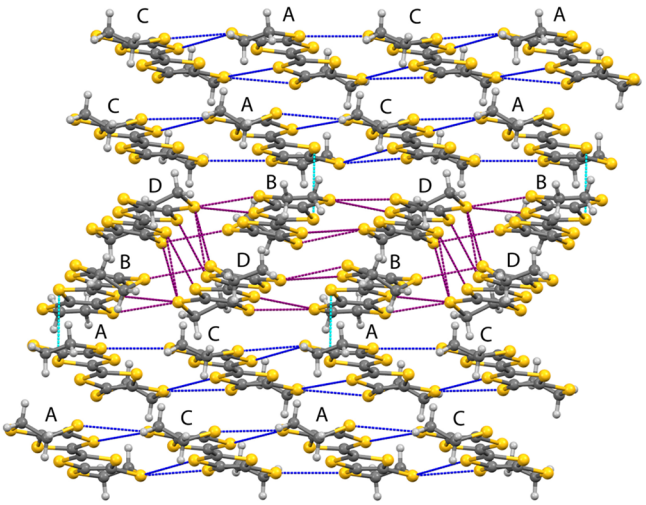

Figure 6. View of the δ-phase packing for **2** where the short intermolecular contacts for the **AA**−**CC** and **BD**−**DB** sublayers are highlighted. Blue, contacts on the **AA**−**CC** layer; purple, contacts on the **BD**−**DB** layer; light blue, contacts between sublayers. (Å): S1A···S2C 3.44, S6C···S7A 3.39, S7A···S8C 3.41, S1C···S2A 3.41, S2A···S3C 3.44, S6A···S7C 3.43, S7C···S8A 3.56, S1B···S2A 3.46, S5B···S8D 3.43, S8D···S7B 3.43, S2B···S1D 3.54, S1D···S4B 3.58, S5D···S8B 3.46, S8B···S7D 3.47.

The analysis of the central C═C and internal C−S bond lengths[11] confirms that **E**, the molecule associated in dimers surrounded by the metal complexes, bears a charge of +1, whereas the molecules arranged in the organic layer (**A**−**D**) are present in a mixed-valence state. The longer C═C and shorter C−S bonds for **A** and **D** when compared to **B** and **C** indicates that the former bear a more positive charge than the latter, but a certain degree of charge delocalization occurs, since **B** and **C** are not in their neutral form (Table 3).

Compound **3** crystallizes in the triclinic centrosymmetric space group $P\bar{1}$ with 18 independent BEDT-TTF molecules (indicated as **A1**, **A2**, **A3**, ..., **F1**, **F2**, **F3**) and three complex anions $[Fe(Cl_2An)_3]^{3-}$ in the asymmetric unit. This compound is isostructural to a recently reported solvate formulated as θ-$[BEDT\text{-}TTF]_6[Fe(Cl_2An)_3]\cdot(H_2O)_{1.5}\cdot(CH_2Cl_2)_{0.5}$ (**3′**).[14] In Figure 7 the crystal packing of **3** is reported, showing organic−inorganic layer segregation as observed in **2**.

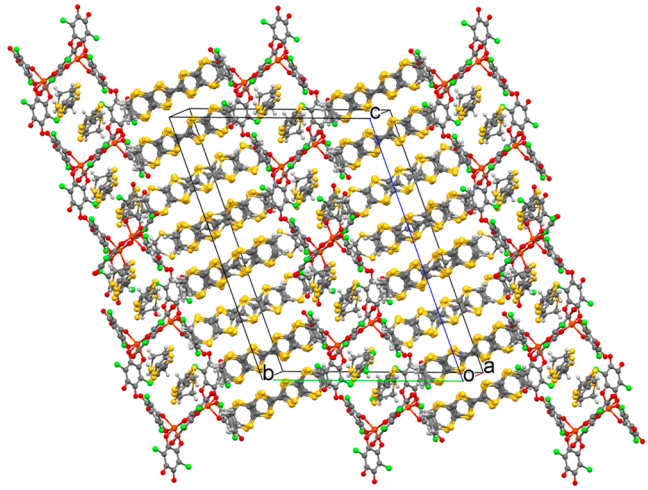

Figure 7. Crystal packing of **3** along the *bc* plane showing the organic−inorganic layer segregation. Crystallization water and CH_2Cl_2 molecules were omitted for clarity.

The hybrid inorganic layer of **3** shows alternated anionic complexes of opposite chirality that surround dimers of mono-oxidized BEDT-TTF radical cations (**F**-type molecules). This packing motif, observed also in **1** and **2** (see Supporting Information, Figure S2), points out the templating influence of the intermolecular interactions between the chloranilate ligand and the dimerized BEDT-TTF molecules.

The organic layer shows donor molecules stacked in the unusual and peculiar α''' structural packing motif.[4c,12] In fact, the BEDT-TTF molecules stack in columns with an arrangement reminiscent of the α structural packing,[12] but with a 2:1:2:1 alternation of the relative disposition of the molecules, instead of the classical 1:1:1:1 sequence (Figure 8). The α''' phase can be regarded as 1:2 hybrid of θ and β'' phases.

Table 3. Bond Distance Analysis and Selected Bond Distances (Å) for the BEDT-TTF Donor Molecules in 2

		A	B	C	D	E
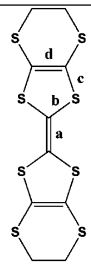	**a**	1.372(10)	1.373(10)	1.343(10)	1.365(10)	1.390(11)
	b	1.737(7)	1.750(7)	1.749(7)	1.724(7)	1.718(9)
		1.734(7)	1.745(7)	1.749(8)	1.747(7)	1.755(8)
		1.721(7)	1.745(7)	1.739(8)	1.742(7)	1.735(9)
		1.740(7)	1.745(7)	1.764(7)	1.744(7)	1.727(9)
	c	1.736(7)	1.749(7)	1.749(7)	1.724(7)	1.718(9)
		1.738(7)	1.748(8)	1.749(8)	1.747(7)	1.755(8)
		1.738(7)	1.748(7)	1.743(8)	1.742(7)	1.735(9)
		1.765(7)	1.755(8)	1.764(7)	1.744(7)	1.727(9)
	d	1.375(10)	1.348(10)	1.340(10)	1.360(10)	1.390(12)
		1.355(10)	1.343(10)	1.338(11)	1.370(10)	1.360(13)
$\delta = (b+c)-(a+d)$	δ	0.740	0.778	0.820	0.748	0.703
$Q = 6.347-7.4638\cdot\delta$	Q	0.8(1)	0.5(1)	0.2(1)	0.8(1)	1.0(1)

dx.doi.org/10.1021/ic501001r | Inorg. Chem. 2014, 53, 7028−7039

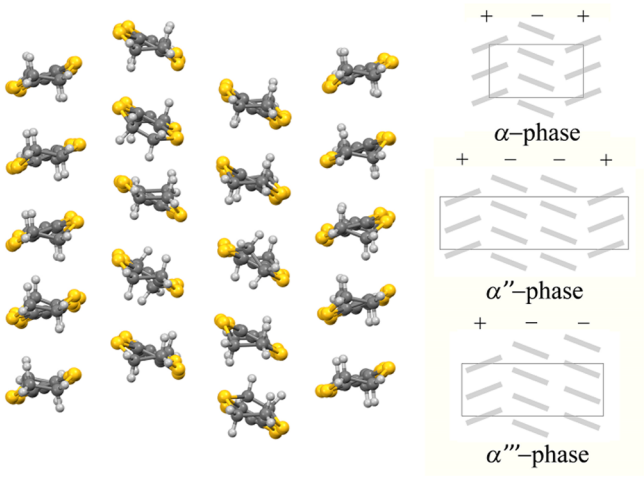

Figure 8. View of α''' packing of **3** along the *ac* plane (left); schematic representation of the BEDT-TTF molecules arranged in the α, α'', and α''' packing motifs (right).

The donors show two different types of interstack S···S contacts; one type (depicted in blue in Figure 9) between

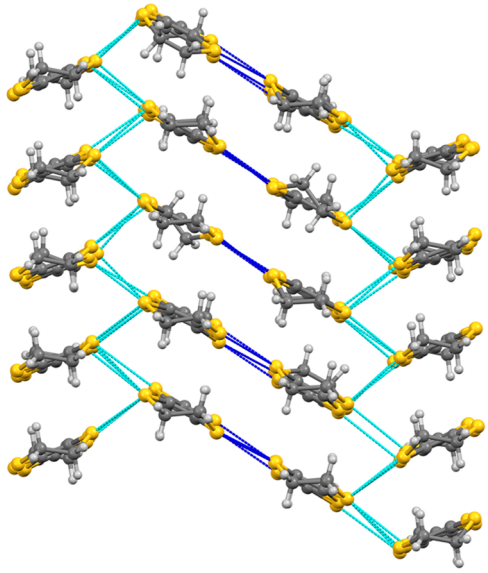

Figure 9. View of the BEDT-TTF packing of **3** along the *ac* plane, where the short intermolecular S···S contacts are highlighted. Some short contacts (Å): S1D1···S7A1 3.40, S7A1···S3D1 3.31, S3A1···S7D1 3.40, S7D1···S1A1 3.39, S1B1···S5C1 3.48, S1D2···S2D1 3.30, S1D2···S2C1 3.49, S1D2···S4D1 3.57, S5D5···S8D1 3.52, S8D1···S7D2 3.42.

columns of BEDT-TTF having the same orientation, in the 3.14−3.48 Å range, and another type (depicted in light blue in Figure 9) between columns of BEDT-TTF having opposite orientation, in the 3.30−3.58 Å range. The former are the strongest in the structure, whereas the intrastack S···S distances are longer than the sum of the van der Waals radii.

The analysis of the central C=C and internal C−S bond lengths[11] confirms that the **F**-type molecules, associated in dimers and surrounded by the metal complexes, each bear a charge of +1, as observed for **1**, **2**, and also for **3**′. The molecules arranged in the organic layer (**A1**, **A2**, **A3**, ..., **E1**, **E2**, **E3**) are, instead, present in a mixed-valence state, with similar values in bond lengths and positive charge associated with each molecule, confirming a certain degree of charge delocalization, as expected for such type of molecular packing (Table 4).

Transport Properties and Band Structure Calculations. The direct current (DC) conductivity measurements in compound **1** show a room-temperature conductivity of ca. 3×10^{-4} S cm^{-1} that decreases as the sample is cooled in a semiconducting way (Figure 10). The Arrhenius plot ($\ln(\rho)$ vs $1/T$) shows a linear behavior that can be fit to an Arrhenius law ($\ln(\rho) = \ln(\rho_0) + E_a/kT$) with an activation energy E_a of ca. 200 meV (inset in Figure 10). This behavior indicates that compound **1** is a semiconductor with low room-temperature conductivity and high activation energy, in agreement with the structural data that show that in this compound all the BEDT-TTF molecules bear a charge of +1, precluding a charge delocalization along the organic layers.

Compounds **2** and **3** show a much higher room-temperature conductivity, between 1 and 10 S cm^{-1} (depending on the quality of the single crystals) with average values of ca. 2 S cm^{-1} (**2**) and 8 S cm^{-1} (**3**) and a semiconducting behavior as shown by the increase of the resistivity as the temperature is decreased (Figure 11). The Arrhenius plot shows that both salts have low activation energies of ca. 700 K (60 meV) and 740 K (64 meV) for **2** and **3**, respectively (inset of Figure 11). The high room-temperature conductivity and low activation energy values for **3** are similar to those found in compound **3**′.[14]

Resistivity measurements were also performed on a second crystal of compound **3** under high hydrostatic pressure. The pressure dependence of the electrical conductivity, $\sigma(P)$, at room temperature is linear, with a slope of $(\sigma(\mathrm{P}) - \sigma(1\ \mathrm{bar}))/\sigma(1\ \mathrm{bar}) = 28\%\ (\mathrm{kbar})^{-1}$ (Supporting Information, Figure S3), in agreement with the low resistivity value and the low activation energy measured at ambient pressure. Moreover, the temperature dependence of the resistivity (Supporting Information, Figure S3) shows that the activation energy is decreasing with the pressure. A value of the order of the temperature (E_a around 300 K) is reached at 12 kbar, indicating that the gap is no more significant.

As mentioned in the structural discussion, there are two very different types of BEDT-TTF molecules in the structure of **2**: those leading to the donor layers (donors **A** to **D**) and those outside the layers, occurring between the anions (donor **E**). Before proceeding to the analysis of the electronic structure we must consider the role of these **E**-type BEDT-TTF donors. They are found as dimers in between the $[Fe(Cl_2An)_3]^{3-}$ anions. Both the S···S distances, which are quite short, and the overlap mode, with sulfur atoms almost on top of each other leading to a strong σ type HOMO···HOMO (HOMO = highest occupied molecular orbital) interaction, suggest that these dimers must be considered as $[(\mathrm{BEDT\text{-}TTF})_2]^{2+}$. This is consistent with the central C=C bond length of donor **E**, 1.381 Å, which is the largest of the system, and the very large splitting (1.29 eV) between the bonding and antibonding combinations of the HOMOs.

The repeat unit of the donor layer contains four different types of BEDT-TTF donors (Figure 12). Consequently, the average charge of these donors is $(2/4)^+$. Since the layers contain eight BEDT-TTF donors, the band structure near the Fermi level will contain eight HOMO-based bands. Because of the stoichiometry these bands must contain four holes so that the equivalent of two of these bands must be empty. The calculated band structure for this salt is shown in Figure 13. There is a band gap of around 35 meV separating the two upper bands from the lower ones so that the conductivity must

dx.doi.org/10.1021/ic501001r | Inorg. Chem. 2014, 53, 7028−7039

Table 4. Bond Distance Analysis and Selected Bond Distances (Å) for some BEDT-TTF Molecules in 3[a]

		A1	B1	C1	D1	E1	F1
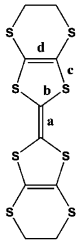	a	1.380(12)	1.393(12)	1.350(12)	1.390(11)	1.355(8)	1.395(9)
	b	1.732(9)	1.710(8)	1.737(8)	1.708(9)	1.728(8)	1.713(8)
		1.755(9)	1.747(8)	1.772(8)	1.753(8)	1.759(8)	1.735(8)
		1.745(9)	1.726(8)	1.746(9)	1.747(8)	1.744(8)	1.720(9)
		1.735(9)	1.731(8)	1.747(9)	1.729(8)	1.743(8)	1.736(9)
	c	1.748(8)	1.740(9)	1.738(8)	1.754(9)	1.756(7)	1.729(9)
		1.754(9)	1.741(8)	1.754(9)	1.745(9)	1.748(9)	1.742(9)
		1.769(8)	1.751(8)	1.755(8)	1.752(8)	1.748(8)	1.720(9)
		1.758(9)	1.756(8)	1.785(8)	1.791(8)	1.760(8)	1.736(9)
	d	1.356(13)	1.363(12)	1.379(12)	1.335(13)	1.347(13)	1.372(11)
		1.333(13)	1.340(12)	1.337(12)	1.335(13)	1.353(12)	1.375(12)
δ = (b+c)-(a+d)	δ	0.775	0.731	0.801	0.770	0.792	0.689
Q = 6.347-7.4638·δ	Q	0.6(1)	0.7(1)	0.4(1)	0.6(1)	0.4(1)	1.1(1)

[a]Note that analyses were performed only on 6 out of 18 crystallographically independent molecules, and the obtained values must be considered as average values.

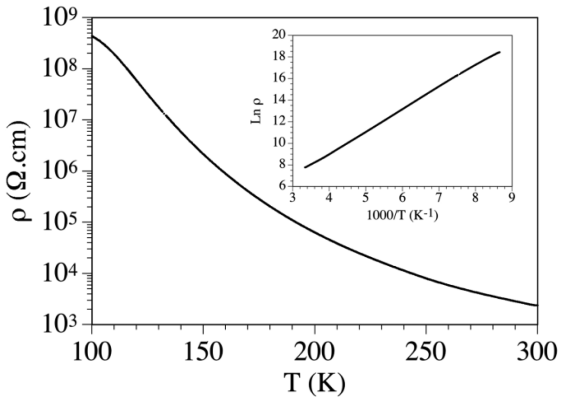

Figure 10. Thermal variation of the electrical resistivity of compound 1. (inset) Arrhenius plot.

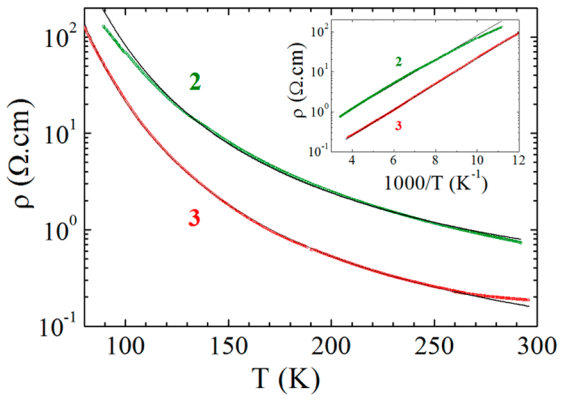

Figure 11. Temperature dependence of the electrical resistivity ρ for single crystals of compounds 2 and 3. (inset) Arrhenius plot. The black lines are the fit to the data with the law $\rho = \rho_0 \exp(E_a/T)$ giving the activation energy E_a.

exhibit an activated behavior, in agreement with the transport measurements.

What is the origin of the activated conductivity? To answer this question we analyzed the density of states of this salt and found that the two upper bands are strongly based on the HOMO levels of donors **A** and **D**, whereas the upper filled level is strongly based on those of the **B** type. To understand this observation, which is at the origin of the gap occurrence, we must have a hint as to the strength of the different HOMO··HOMO interactions, which ultimately dictate the composition and shape of the HOMO bands. The repeat unit of the layers

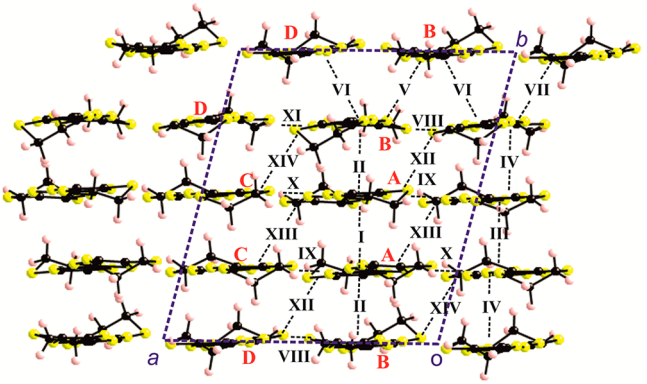

Figure 12. Donor layer of compound 2 where the four different donors and 14 intermolecular interactions are shown.

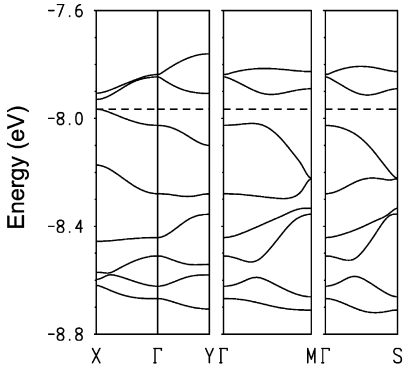

Figure 13. Calculated band structure for the donor layers of 2 where Γ = (0, 0), X = (a*/2, 0), Y = (0, b*/2), M = (a*/2, b*/2) and S = (−a*/2, b*/2). The dashed line refers to the highest occupied level.

contains 14 different intermolecular interactions (see Figure 12 for the labeling). The strength of the HOMO···HOMO interactions associated with the different intermolecular interactions may be quantified from their associated $|\beta_{HOMO-HOMO}|$ interaction energies.[15] The calculated values for the present salt are reported in Table 5. An important observation is that all the values corresponding to lateral interactions (VIII to XI) as well as XII−XIV and VI are smaller (between 0.0635 and 0.1640) than those from I to IV as well as V and VII (between 0.2016 and 0.3587). This means that the HOMO···HOMO interactions within the chains **−B−A−A−B−B−A−A−B−** and **−D−C−C−D−D−C−C−D−** along the b direction play the leading role in building the bands of Figure

dx.doi.org/10.1021/ic501001r | Inorg. Chem. 2014, 53, 7028−7039

Table 5. $|\beta_{HOMO-HOMO}|$ Interaction Energies (eV) for the Donor···Donor Interactions Defined in Figure 12

interaction		$\|\beta_{HOMO-HOMO}\|$	interaction		$\|\beta_{HOMO-HOMO}\|$
I	(A−A)	0.3587	II	(A−B)	0.3296
III	(C−C)	0.2383	IV	(C−D)	0.2016
V	(B−B)	0.3094	VI	(B−D)	0.0849
VII	(D−D)	0.3282	VIII	(B−D)	0.1153
IX	(A−C)	0.1593	X	(A−C)	0.1499
XI	(B−D)	0.1212	XII	(A−D)	0.0608
XIII	(C−A)	0.1640	XIV	(B−C)	0.0635

13. As far as the second chain is concerned, the **D**−**D** interaction (VII) is by far the strongest. This means that the antibonding combination of the two HOMOs of the **D**-type BEDT-TTFs will provide the highest lying levels of this chain and thus will be the major building blocks of one of the empty bands in Figure 13. In the first chain, the **A**−**A** interaction (I) is still the strongest, but the difference with interaction **A**−**B** (II) is smaller. Consequently, although the higher-lying levels associated with this chain, that is, the second, lower empty band, will be based on the antibonding combination of the HOMOs of the **A**-type BEDT-TTFs they will also contain substantial contributions from the **B**-type BEDT-TTFs. However, if the interactions coupling the chains are considered, those associated with the **A** donors (0.1640, 0.1593, 0.1499 and 0.0608) are stronger than those associated with the **B** ones (0.1212, 0.1153, 0.0849 and 0.0635). This means that the antibonding interchain interactions affect more strongly the HOMO-**A** levels and, as a result, the levels of the second empty band are relocalized on the local **A**−**A** dimers.

Thus, the **A**−**A** and **D**−**D** dimerizations, by leading to high energy lying antibonding combinations of the HOMOs located on these dimers, provide the main driving force for the occurrence of a band gap in this salt. Since the dimerization is already strong in the **−D−C−C−D−D−C−C−D−** chain and thus leads to the upper empty band, it is the **−B−A−A−B−B−A−A−B−** chain that mostly controls the magnitude of the gap. There are two ways to increase/(decrease) the dimerization and thus the band gap: (i) decreasing/(increasing) the intrachain **A**−**B** interaction, and (ii) increasing/(decreasing) the strength of the HOMO···HOMO interchain interactions associated with donors **A** with respect those affecting donors **B**.

The repeat unit of compound **3** contains 18 different types of BEDT-TTF donors. Fifteen of them (**A1**, **A2**, **A3**,.... **E1**, **E2**, **E3**) lead to the donor layers and three of them (**F1**, **F2**, **F3**) are found in between these donor layers in the vicinity of the anions. The repeat unit of the layers contains 30 BEDT-TTF donors, and there are 45 different intermolecular interactions. Thus, calculating and understanding the band structure of this material is a truly challenging task. Before trying to solve this problem we must consider the role of the **F**-type BEDT-TTF donors. These donors are found as two different types of dimers in between the $[Fe(Cl_2An)_3]^{3-}$ anions. Both the S···S distances, which are short, and the $|\beta_{HOMO-HOMO}|$ interaction energies, which are by far the largest ones (0.6390 and 0.5060 eV) of the system (see below), suggest that these dimers are really $[(BEDT\text{-}TTF)_2]^{2+}$ as is also the case for compound **2**. Thus, in terms of electron counting, the **F**-type donors should be considered as bearing a positive charge so that the average charge of the 15 symmetry nonequivalent BEDT-TTF donors of the layer is $(6/15)^+$.

The many intermolecular interactions in the layer can be divided into three different groups: (i) those within the chains along *a*, (ii) those between pairs of chains of donors with the same inclination with respect to the *a* direction, and (iii) those between pairs of chains of donors with opposite inclination with respect to the *a* direction. The shortest S···S contacts are associated with the second ones. However, most of the physical properties of molecular conductors are determined by the band structure near the Fermi level and, thus, by the strength of the HOMO···HOMO interactions. The calculated values of the $|\beta_{HOMO-HOMO}|$ interaction energies for the present salt occur in a range between 0.05 and 0.17 eV for the interactions (i) and between 0.03 and 0.18 for those of type (iii). The strongest interactions are those between pairs of chains with the same inclination with respect to *a*. However, among them, the interactions between pairs of donors approximately in the same plane (i.e., those associated with the dark blue interactions in Figure 9), which are associated with the shortest S···S contacts in the structure, are only associated with $|\beta_{HOMO-HOMO}|$ values of ∼0.15 eV, whereas those not highlighted in Figure 9 are the largest in the layer, ∼0.30−0.35 eV. The reason why the first are smaller is that the contacts are lateral with π type overlaps, which are generally weak. In contrast, the latter have a strong σ-type component because of the favorable orientation of the S p_z orbitals. Globally, the strongest interactions in the layer are those between the pairs of donors with the same inclination that form a continuous zigzag path along the *a* direction. However, these zigzag chains of interactions are connected through the numerous interactions of type (ii), which even if smaller are by no means negligible, so that we conclude that **3** should be a 2D conductor although with somewhat better conductivity along *a*, that is, the chain direction. This is in contrast with most α-type salts, for instance, those of the well-known α-$(BEDT\text{-}TTF)_2MHg(SCN)_4$ (M = K, Rb, Tl, NH_4) family,[16] which are 2D conductors with better conductivity in the direction perpendicular to the chains.

The donor layers of **3** contain 30 BEDT-TTF donors, and consequently, the band structure near the Fermi level will contain 30 HOMO-based bands. Taking into account the above-mentioned average charge of the layer donors, these bands must contain 12 holes so that the equivalent of six of these bands must be empty. From the viewpoint of the correlation between the electronic structure and conductivity of the system there are two different possibilities: (i) there is a band gap separating the six upper HOMO-based bands from the lower ones so that the system will exhibit an activated conductivity; (ii) there is no band gap separating the six upper bands form the lower ones, and then the system is either metallic or semiconducting when disorder is strong enough to localize the carriers. Thus, it is very important to establish if a band gap really occurs for the appropriate electron count in the band structure. We have succeeded in calculating the band structure for this very large system, and the 15 upper HOMO bands are shown in Figure 14. The important observation is that the top of the upper filled band, noted as a dashed line in Figure 14, is separated by an indirect band gap of approximately 10 meV from the bottom of the next band. Inspection of the full Brillouin zone confirms this observation. Consequently, as is the case for **2**, compound **3** is a regular semiconductor with a small band gap and thus with a relatively high, though activated, conductivity. Analysis of the topology of the calculated band structure does not provide a better insight than that provided by consideration of the different $|\beta_{HOMO-HOMO}|$ values (see

dx.doi.org/10.1021/ic501001r | Inorg. Chem. 2014, 53, 7028−7039

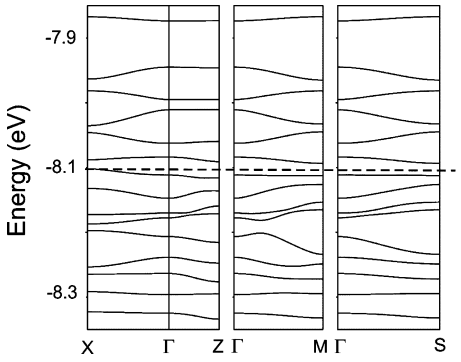

Figure 14. Upper 15 HOMO-based bands calculated for the donor layers of compound **3** where Γ = (0, 0), X = (a*/2, 0), Z = (0, c*/2), M = (a*/2, c*/2), and S = (−a*/2, c*/2). The dashed line refers to the upper filled level.

above). The large number of bands and symmetry nonequivalent molecules together with the low symmetry of the lattice lead to a plethora of avoided crossings between bands. The band structure thus appears as a large series of quite flat bands, most of them being separated from each other with relatively small gaps. We suspect that this will be the case for most of the molecular conducting salts with such large number of independent donors, which most likely will exhibit a semiconducting behavior.

Magnetic Measurements. The thermal variation of the product of the magnetic susceptibility times the temperature ($\chi_m T$) for compound **1** shows a room-temperature value of ca. 4.75 cm^3 K mol^{-1}, slightly above the expected value for one isolated Fe(III) S = 5/2 ion (4.375 cm^3 K mol^{-1}). When the temperature is decreased, $\chi_m T$ shows a smooth decrease and reaches a plateau of ca. 4.45 cm^3 K mol^{-1} below ca. 60 K. Below ca. 10 K $\chi_m T$ shows a more abrupt decrease and reaches a value of ca. 3.95 cm^3 K mol^{-1} at 2 K (Figure 15). This behavior

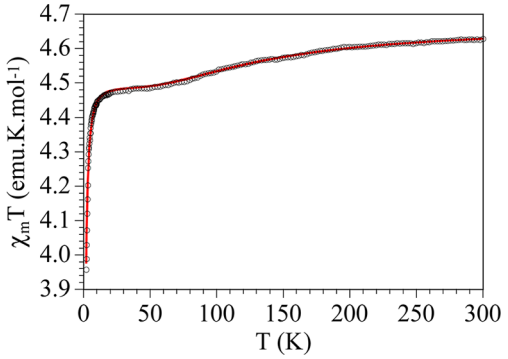

Figure 15. Thermal variation of the $\chi_m T$ product for compound **1**. Solid line is the best fit to the model (see text).

indicates that besides the expected contribution from the $[Fe(Cl_2An)_3]^{3-}$ anions, at high temperature there is an extra contribution from the BEDT-TTF sublattice of ca. 0.3 cm^3 K mol^{-1}, which is close to the expected contribution of one unpaired localized electron. Since there are three BEDT-TTF$^{+\bullet}$ radicals per formula unit, we can assume that two of the three radicals are strongly antiferromagnetically coupled and, therefore, do not present any contribution to the magnetic moment. A close look at the S···S intermolecular contacts indicates that most probably the dimer **AB** is the one presenting a strong AF coupling, since it shows several intermolecular S···S interactions in the range of 3.43−3.49 Å, much shorter than the sum of the van der Waals radii (3.65 Å). The other dimer (**CC**) presents larger intermolecular S···S contacts (in the range of 3.48−3.57 Å) and, therefore, it would be responsible for the extra contribution and the observed AF coupling. This assumption agrees with the fact that there is half **CC** dimer (i.e., one electron) and one **AB** dimer per formula unit. The abrupt decrease observed at very low temperatures is attributed to the presence of a zero field splitting (ZFS) of the S = 5/2 Fe(III) ion. Accordingly, we have fitted the magnetic properties of compound **1** to a model including the contribution of an isolated S = 5/2 ion with a ZFS and that of a half S = 1/2 dimer with an AF coupling. To reduce the number of adjustable parameters, we have fixed the g value of the BEDT-TTF radicals to 2.0. This model reproduces very satisfactorily the magnetic properties of compound **1** (solid line in Figure 15) with g_{Fe} = 2.026, $|D|$ = 1.2 cm^{-1}, $g_{BEDT\text{-}TTF}$ = 2.0 (fixed), and J_{CC} = −180 cm^{-1} (J_{CC} is the intradimer coupling constant. The Hamiltonian is written as $H = -JS_1S_2$). Note that it is not possible to determine the sign of D from powder magnetic measurements and that the obtained D value could also contain a very weak antiferromagnetic interaction.

The D value is in good agreement with the reported value for this magnetic building block as $[PPh_4]^+$ salt[9] and within the normal range found in many Fe(III) complexes with similar structures.[17]

EPR Spectroscopy. The electron paramagnetic resonance (EPR) spectra of a single crystal of compound **3** for any orientation shows a single line (Supporting Information, Figure S4) with a line-width of 26 G when the magnetic field is perpendicular to the plane of the BEDT-TTF molecules in the organic layer and 33 G when the field is parallel to the BEDT-TTF molecular plane (Supporting Information, Figures S4 and S5). The g values oscillate between 2.003 and 2.011 for the perpendicular and parallel orientations, respectively (Supporting Information, Figure S5). These values are within the normal range found in many other BEDT-TTF salts.[1f] The intensity of this signal slightly decreases when the temperature is decreased for both orientations of the magnetic field: parallel (θ = 0°, Supporting Information, Figure S6) or perpendicular to the layers (θ = 90°, Supporting Information, Figure S7), suggesting the presence of an antiferromagnetic coupling between the BEDT-TTF radicals. In fact, the thermal variation of the normalized product of the spin susceptibility (proportional to the area of the signal) times the temperature ($\chi_s T$) shows a continuous decrease when the temperature is lowered and approaches zero at very low temperatures, confirming the AF coupling in the cationic lattice (Figure 16).

The g and ΔH values also decrease when the sample is cooled (inset in Figure 16), although at very low temperatures it is very difficult to measure the signal since it is masked by a large signal arising from the Fe(III) anions whose intensity increases as the sample is cooled, as expected for a paramagnetic Fe(III) anion (Supporting Information, Figures S6 and S7).

CONCLUSIONS

Three different crystalline radical cation salts based on the BEDT-TTF donor and the tris(chloranilato)ferrate(III) anion were prepared via electrocrystallization by slightly changing the stoichiometry donor/anion and the solvents. As a common structural feature for the three phases one can disclose the presence of dimerized oxidized BEDT-TTF units in the

dx.doi.org/10.1021/ic501001r | Inorg. Chem. 2014, 53, 7028−7039

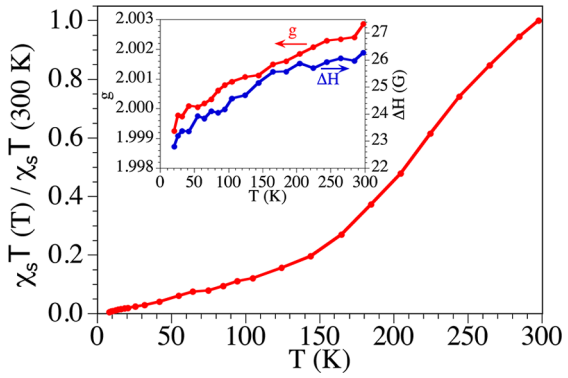

Figure 16. Thermal variation of the normalized $\chi_s T$ product of the X-band EPR signal of compound **3** when the magnetic field is parallel to the layers ($\theta = 0°$). (inset) Thermal variation of the g value (left scale) and line width (ΔH, right scale) in the same experiment.

inorganic layer, very likely thanks to the establishment of intermolecular S···Cl contacts and also electrostatic interactions. While in compound **1**, of 3:1 stoichiometry, the three BEDT-TTF molecules are fully oxidized in radical cations, in the salts **2** and **3**, of 5:1 and 6:1 stoichiometry, respectively, only the donors located in the inorganic layers are fully oxidized, while those forming the organic slabs are in mixed valence state. The packing motif found in the organic layers is of δ type in **2** and α''' type in **3**. Single-crystal conductivity measurements show semiconducting behavior for the three materials, but with low room-temperature conductivity and high activation energy for **1**, as expected from the structural analysis, and high room-temperature conductivity of 1−10 S cm^{-1} for **2** and **3**, with low activation energies of 60−65 meV. Band structure calculations for **2** and **3** are in agreement with an activated conductivity with low band gaps. A detailed analysis of the density of states and HOMO···HOMO interactions in **2** explains the origin of the gap as a consequence of a dimerization in one of the donor chains, whereas the challenging calculation of **3**, due to the presence of 18 crystallographically independent BEDT-TTF molecules, represents a milestone in the band structure calculations of such relatively rare and complex crystal structures. Magnetic susceptibility measurements for **1** clearly indicate the presence of isolated high spin $S = 5/2$ Fe(III) ions, with a contribution at high temperatures from BEDT-TTF radical cations. These latter are evidenced also by EPR variable-temperature measurements on single crystals of **3**. This first family of conducting radical cation salts based on the magnetic tris(chloranilato)-ferrate(III) complex demonstrates the versatility of this type of anion for the preparation of multifunctional molecular materials. As perspective, a topic of current special interest is the introduction of chirality in the organic layer,[18] thus allowing for the preparation of multifunctional materials in which the chirality may influence the conducting properties.

EXPERIMENTAL SECTION

General. $[PPh_4]_3[Fe(Cl_2An)_3]$ was synthesized according to the literature procedure.[9] BEDT-TTF (Aldrich) was used as received. Crystals were grown by the electrocrystallization technique.[19] Solvents used for electrocrystallization experiments (HPLC grade) were dried under basic alumina and degassed with argon prior to use.

Syntheses. *$[BEDT\text{-}TTF]_3[Fe(Cl_2An)_3]\cdot 3CH_2Cl_2\cdot H_2O$ (**1**).* $[PPh_4]_3[Fe(Cl_2An)_3]$ (22 mg) was dissolved in 8 mL of CH_2Cl_2 and placed in the cathode chamber of an H-shape electrocrystallization cell. BEDT-TTF (5 mg) was dissolved in 8 mL of CH_2Cl_2 and placed in the anode chamber of the cell. A current density of 1.0 μA cm^{-2} was applied. Black prismatic single crystals of **1** were grown at 20 °C on the anode surface of a platinum wire electrode over a period of one month.

*δ-$[BEDT\text{-}TTF]_5[Fe(Cl_2An)_3]\cdot 4H_2O$ (**2**).* $[PPh_4]_3[Fe(Cl_2An)_3]$ (6 mg) was dissolved in 8 mL of CH_3CN and placed in the cathode chamber of an H-shape electrocrystallization cell. BEDT-TTF (3 mg) was dissolved in 8 mL of CH_3CN and placed in the anode chamber of the cell. A current density of 1.0 μA cm^{-2} was applied. Single crystals of **2** as black thin plates were grown at 20 °C on the anode surface of a platinum wire electrode over a period of three weeks.

*α'''-$[BEDT\text{-}TTF]_{18}[Fe(Cl_2An)_3]_3\cdot 3CH_2Cl_2\cdot 6H_2O$ (**3**).* $[PPh_4]_3[Fe(Cl_2An)_3]$ (6 mg) was dissolved in 8 mL of a 1:1 CH_2Cl_2/CH_3CN

Table 6. Summary of X-ray Crystallographic Data for 1, 2, and 3

	1	2	3
empirical formula	$C_{51}H_{30}Cl_{12}FeO_{13}S_{24}$	$C_{68}H_{40}Cl_6FeO_{16}S_{40}$	$C_{237}H_{150}Cl_{24}Fe_3O_{42}S_{144}$
formula weight	2101.44	2663.95	9304.56
crystal size, mm	0.40 × 0.20 × 0.05	0.33 × 0.27 × 0.13	0.14 × 0.09 × 0.05
crystal system	triclinic	triclinic	triclinic
space group	$P\bar{1}$	$P\bar{1}$	$P\bar{1}$
a, Å	13.177(1)	13.382(1)	20.944(1)
b, Å	15.356(2)	16.152(2)	26.679(1)
c, Å	19.795(2)	24.269(2)	33.931(1)
α, deg	92.030(7)	104.052(8)	68.231(2)
β, deg	106.571(6)	93.403(7)	80.742(2)
γ, deg	96.654(7)	101.751(7)	71.238(2)
V, Å^3	3803(1)	4949(1)	16654(1)
Z	2	2	2
T, K	293(2)	150(2)	293(2)
ρ (calc), Mg/m^3	1.835	1.788	1.856
μ, mm^{-1}	1.337	1.219	1.291
θ range, deg	1.66 to 27.01	1.56 to 26.50	1.55 to 26.00
GOF	1.037	1.079	1.041
$R1^a$	0.0700	0.1065	0.1202
$wR2^a$	0.1772	0.2738	0.2970

$^a R1 = \Sigma||F_o| - |F_c||/\Sigma|F_o|$, $wR2 = [\Sigma[w(F_o^2 - F_c^2)^2]/\Sigma[w(F_o^2)^2]]^{1/2}$ $w = 1/[\sigma^2(F_o^2) + (aP)^2 + bP]$, where $P = [\max(F_o^2,0) + 2F_c^2]/3$.

dx.doi.org/10.1021/ic501001r | Inorg. Chem. 2014, 53, 7028−7039

mixture and placed in the cathode chamber of an H-shape electrocrystallization cell. BEDT-TTF (3 mg) was dissolved in 8 mL of a 1:1 CH_2Cl_2/CH_3CN solution and placed in the anode chamber of the cell. A current density of 1.0 μA cm^{-2} was applied. Single crystals of **3** as black elongated prisms were grown at 20 °C on the anode surface of a platinum wire electrode over a period of one week.

X-ray Crystallography. X-ray diffraction measurements were performed on a Nonius Kappa CCD diffractometer, using graphite-monochromated Mo Kα radiation (λ = 0.710 73 Å). The structures were solved by direct methods (SHELXS-97) and refined on F^2 with full-matrix least-squares (SHELXL-97),[20] using the Wingx software package.[21] The non-H atoms were refined with anisotropic displacement parameters. The crystallization water molecules were refined without the hydrogen atoms. A summary of the crystallographic data and the structure refinement for **1**−**3** is reported in Table 6. Crystallographic data for the structures were deposited in the Cambridge Crystallographic Data Centre (see Supporting Information).

Single-Crystal Conductivity Measurements. The single-crystal conductivity measurements were carried out with the four or two contacts methods (depending on the size of the single crystals) on six different single crystals of compound **1** in the temperature range of 300−2 K (although the resistance was above our detection limit below ca. 110 K). The results were identical in the cooling and warming scans. The contacts were made with Pt wires (25 μm diameter) using graphite paste. The samples were measured in a Quantum Design PPMS-9 equipment connected to an external voltage source (Keithley model 2400 source-meter) and amperometer (Keithley model 6514 electrometer). The samples were measured by applying a constant voltage of 1 V and measuring the intensity. All the conductivity quoted values were measured in the voltage range where the crystals are Ohmic conductors. Below ca. 110 K the resistance becomes higher than the detection limit of our equipment. The cooling and warming rates were 0.5 K/min in all cases. For compounds **2** and **3** electrical resistivity was measured on platelet-shaped single crystals using a four-point method. Four gold contacts were evaporated on both faces of the crystals, and gold wires (17 mm diameter) were glued with silver paste on those contacts. A low-frequency (<100 Hz) lock-in technique was used with a measuring current I_{ac} = 0.1 μA. Low temperature, in the range of 15−300 K, was provided by a cryocooler equipment. Experiments under high hydrostatic pressure were performed in a CuBe clamped cell up to 12 kbar with silicon oil (Daphne 7373) as pressure transmitting medium. The pressure at room temperature was extracted from the resistance of a manganin gauge in the pressure cell, and it is this value that is indicated in the figures. However, the loss of pressure during cooling is estimated to 2 kbar. A copper-constantan thermocouple inside the pressure cell was used as the thermometer.

EPR Measurements. The EPR spectra were recorded on a single crystal of compound **3** from 2900 to 3900 G in the temperature range of 300−5 K with an X-band (9.48 GHz) Bruker ELEXSYS E580 Spectrometer equipped with a helium cryostat. The crystal was rotated along the longitudinal axis so that the field was parallel or perpendicular to the layers for θ values of 0° or 90°, respectively.

Band Structure Calculations. The tight-binding band structure calculations were of the extended Hückel type.[22] A modified Wolfsberg−Helmholtz formula[23] was used to calculate the non-diagonal $H_{\mu\nu}$ values. All valence electrons were taken into account in the calculations, and the basis set consisted of Slater-type orbitals of double-ζ quality for C 2s and 2p, S 3s and 3p, and of single-ζ quality for H. The ionization potentials, contraction coefficients, and exponents were taken from previous work.[24]

Magnetic Measurements. Susceptibility measurements were carried out in the temperature range of 2−300 K with an applied magnetic field of 0.1 T on a polycrystalline sample of compound **1** (mass = 16.03 mg) with a Quantum Design MPMS-XL-5 SQUID susceptometer. The susceptibility data were corrected for the sample holders previously measured using the same conditions and for the diamagnetic contributions of the salt as deduced by using Pascal's constants tables (χ_{dia} = −1077 × 10^{-6} cm^3 mol^{-1}).[25]

■ ASSOCIATED CONTENT

Ⓢ Supporting Information

X-ray crystallographic file in CIF format, additional Figures and Tables as mentioned in the text. This material is available free of charge via the Internet at http://pubs.acs.org. Crystallographic data for the structures was deposited in the Cambridge Crystallographic Data Centre, deposition numbers CCDC 996582 (**1**), CCDC 996583 (**2**), CCDC 996584 (**3**). These data can be obtained free of charge from The Cambridge Crystallographic Data Centre via www.ccdc.cam.ac.uk/data_request/cif.

■ AUTHOR INFORMATION

Corresponding Authors

*E-mail: narcis.avarvari@univ-angers.fr. Fax: (+33)02 41 73 54 05. Phone: (+33)02 41 73 50 84.

*E-mail: mercuri@unica.it. Fax: (+39)0706754486. Phone: (+39)0706754486.

Notes

The authors declare no competing financial interest.

■ ACKNOWLEDGMENTS

This work was supported in France by the CNRS, the University of Angers, and the National Agency for Research (ANR) (ANR Inter, ANR-12-IS07-0004-04, CREMM project). The work in Italy was supported by Regione Autonoma della Sardegna (L.R. 7-8-2007, Bando 2009, CRP-17453 Project "Nano Materiali Multifunzionali per Applicazioni nell'Elettronica Molecolare"), Fondazione Banco di Sardegna, and INSTM. Work at Bellaterra was supported by MINECO (Grant Nos. CSD2007-00041 and FIS2012-37549-C05-05). We also thank the EU (SPINMOL ERC Adv. Grant), the Spanish MINECO (Projects CSD2007-00010 and CTQ-2011-26507), and the Generalitat Valenciana (Prometeo and ISIC-Nano programs) for financial support.

■ REFERENCES

(1) (a) Coronado, E.; Day, P. *Chem. Rev.* **2004**, *104*, 5419−5448. (b) Enoki, T.; Miyazaki, A. *Chem. Rev.* **2004**, *104*, 5449−5478. (c) Kobayashi, H.; Cui, H. B.; Kobayashi, A. *Chem. Rev.* **2004**, *104*, 5265−5288. (d) Mercuri, M. L.; Deplano, P.; Serpe, A.; Artizzu, F. Chapter 7. In *Handbook of Multifunctional Molecular Materials, Multifunctional Nanomaterials of interest in Electronics;* 219−280; Ouahab, L., Ed.; Pan Stanford Publishing: Singapore, 2013. (e) Focused Issue on Molecular Electronics , *Nat. Nanotechnol.* **2013**, *8*, 377−467. (f) Williams, J. M.; Ferraro, J. R.; Thorn, R. J.; Carlson, K. D.; Geiger, U.; Wang, H. H.; Kini, A. M.; Whangbo, M. H. *Organic Superconductors: Synthesis, Structure, Properties and Theory;* Grimes, R. N., Ed.; Prentice Hall: Englewood Cliffs, NJ, 1992. (g) Coronado, E.; Giménez-Saiz, C.; Gómez-García, C. J. *Coord. Chem. Rev.* **2005**, *249*, 1776−1796. (h) Coronado, E.; Clemente-León, M.; Galán-Mascarós, J. R.; Giménez-Saiz, C.; Gómez-García, C. J.; Martínez-Ferrero, E. *J. Chem. Soc., Dalton Trans.* **2000**, 3955−3961.

(2) (a) Kurmoo, M.; Graham, A. W.; Day, P.; Coles, S. J.; Hursthouse, M. B.; Caulfield, J. L.; Singleton, J.; Pratt, F. L.; Hayes, W.; Ducasse, L.; Guionneau, P. *J. Am. Chem. Soc.* **1995**, *117*, 12209−12217. (b) Martin, L.; Turner, S. S.; Day, P.; Mabbs, F. E.; McInnes, E. J. L. *Chem. Commun.* **1997**, *15*, 1367−1368. (c) Rashid, S.; Turner, S. S.; Day, P.; Howard, J. A. K.; Guionneau, P.; McInnes, E. J. L.; Mabbs, F. E.; Clark, R. J. H.; Firth, S.; Biggs, T. *J. Mater. Chem.* **2001**, *11*, 2095−2101. (d) Schlueter, J. A.; Geiser, U.; Whited, M. A.; Drichko, N.; Salameh, B.; Petukhov, K.; Dressel, M. *Dalton Trans.* **2007**, 2580−2588 and references therein.

(3) (a) Uji, S.; Shinagawa, H.; Terashima, T.; Yakabe, T.; Terai, Y.; Tokumoto, M.; Kobayashi, A.; Tanaka, H.; Kobayashi, H. *Nature*

2001, *410*, 908−910. (b) Fujiwara, H.; Fujiwara, E.; Nakazawa, Y.; Narymbetov, B. Zh.; Kato, K.; Kobayashi, H.; Kobayashi, A.; Tokumoto, M.; Cassoux, P. *J. Am. Chem. Soc.* **2001**, *123*, 306−314. (c) Coronado, E.; Falvello, L. R.; Galán-Mascarós, J. R.; Giménez-Saiz, C.; Gómez-García, C. J.; Lauhkin, V. N.; Pérez-Benítez, A.; Rovira, C.; Veciana. *Adv. Mater.* **1997**, *9*, 984−987. (d) Yamaguchi, K.; Kitagawa, Y.; Onishi, T.; Isobe, H.; Kawakami, T.; Nagao, H.; Takamizawa, S. *Coord. Chem. Rev.* **2002**, *226*, 235−249 and references therein. (e) Day, P.; Kurmoo, M.; Mallah, T.; Marsden, I. R.; Friend, R. H.; Pratt, F. L.; Hayes, W.; Chasseau, D.; Gaultier. *J. Am. Chem. Soc.* **1992**, *114*, 10722−10729.

(4) (a) Coronado, E.; Curreli, S.; Giménez-Saiz, C.; Gómez-García, C. J. *J. Mater. Chem.* **2005**, *15*, 1429−1436. (b) Coronado, E.; Curreli, S.; Giménez-Saiz, C.; Gómez-García, C. J. *Inorg. Chem.* **2012**, *51*, 1111−1126. (c) Martin, L.; Day, P.; Clegg, W.; Harrington, R. W.; Horton, P. N.; Bingham, A.; Hursthouse, M. B.; McMilland, P.; Firth, S. *J. Mater. Chem.* **2007**, *17*, 3324−3329. (d) Coronado, E.; Curreli, S.; Giménez-Saiz, C.; Gómez-García, C. J.; Alberola, A. *Inorg. Chem.* **2006**, *45*, 10815−10824.

(5) (a) Tamaki, H.; Zhong, Z. J.; Matsumoto, N.; Kida, S.; Koikawa, M.; Achiwa, N.; Hashimoto, Y.; Okawa, H. *J. Am. Chem. Soc.* **1992**, *114*, 6974−6979. (b) Mathonière, C.; Nuttall, C. J.; Carling, S. G.; Day, P. *Inorg. Chem.* **1996**, *35*, 1201−1206. (c) Coronado, E.; Galan-Mascaros, J. R.; Gomez-Garcia, C. J.; Laukhin, V. *Nature* **2000**, *408*, 447−449. (d) Alberola, A.; Coronado, E.; Galán-Mascarós, J. R.; Giménez-Saiz, C.; Gómez-García, C. J. *J. Am. Chem. Soc.* **2003**, *125*, 10774−10775. (e) Coronado, E.; Galán-Mascarós, J. R.; Gómez-García, C. J.; Martínez-Ferrero, E.; van Smaalen, S. *Inorg. Chem.* **2004**, *43*, 4808−4810. (f) Alberola, A.; Coronado, E.; Galán-Mascarós, J. R.; Giménez-Saiz, C.; Gómez-García, C. J.; Martínez-Ferrero, E.; Murcia-Martínez, A. *Synth. Met.* **2003**, *135*, 687−689.

(6) Fourmigué, M.; Batail, P. *Chem. Rev.* **2004**, *104*, 5379−5418.

(7) (a) Coronado, E.; Curreli, S.; Giménez-Saiz, C.; Gómez-García, C. J.; Deplano, P.; Mercuri, M. L.; Serpe, A.; Pilia, L.; Faulmann, C.; Canadell, E. *Inorg. Chem.* **2007**, *46*, 4446−4457. (b) Gómez-García, C. J.; Coronado, E.; Curreli, S.; Giménez-Saiz, C.; Deplano, P.; Mercuri, M. L.; Pilia, L.; Serpe, A.; Faulmann, C.; Canadell, E. *Chem. Commun.* **2006**, 4931−4933.

(8) (a) Kitagawa, S.; Kawata, S. *Coord. Chem. Rev.* **2002**, *224*, 11−34 and references therein. (b) Tinti, F.; Verdaguer, M.; Kahn, O.; Savariault, J. M. *Inorg. Chem.* **1987**, *26*, 2380−2384. (c) Min, K. S.; Rhinegold, A. L.; Miller, J. S. *J. Am. Chem. Soc.* **2005**, *128*, 40−41. (d) Min, K. S.; Rheingold, A. L.; DiPasquale, A.; Miller, J. S. *Inorg. Chem.* **2006**, *45*, 6135−6137. (e) Min, K. S.; DiPasquale, A. G.; Golen, J. A.; Rheingold, A. L.; Miller, J. S. *J. Am. Chem. Soc.* **2007**, *129*, 2360−2368. (f) Nagayoshi, K.; Kabir, M. K.; Tobita, H.; Honda, K.; Kawahara, M.; Katada, M.; Adachi, K.; Nishikawa, H.; Ikemoto, I.; Kumagai, H.; Hosokoshi, Y.; Inoue, K.; Kitagawa, S.; Kawata, S. *J. Am. Chem. Soc.* **2003**, *125*, 221−232.

(9) Atzori, M.; Artizzu, F.; Sessini; Marchiò, L.; Loche, D.; Serpe, A.; Deplano, P.; Concas, G.; Pop, F.; Avarvari, N.; Mercuri, M. L. *Dalton Trans.* **2014**, *43*, 7006−7019.

(10) Atzori, M.; Benmansour, S.; Mínguez Espallargas, G.; Clemente-León, M.; Abhervé, A.; Gómez-Claramunt, P.; Coronado, E.; Artizzu, F.; Sessini, E.; Deplano, P.; Serpe, A.; Mercuri, M. L.; Gómez García, C. J. *Inorg. Chem.* **2013**, *52*, 10031−10040.

(11) Guionneau, P.; Kepert, C. J.; Bravic, G.; Chasseau, D.; Truter, M. R.; Kurmoo, M.; Day, P. *Synth. Met.* **1997**, *86*, 1973−1974.

(12) (a) Mori, T. *Bull. Chem. Soc. Jpn.* **1998**, *71*, 2509−2526. (b) Mori, T. *Bull. Chem. Soc. Jpn.* **1999**, *72*, 2011−2027. (c) Mori, T.; Mori, H.; Tanaka, S. *Bull. Chem. Soc. Jpn.* **1999**, *72*, 179−197. (d) Shibaeva, R. P.; Yagubskii, E. B. *Chem. Rev.* **2004**, *104*, 5347−5378.

(13) (a) Clemente-León, M.; Coronado, E.; Gómez-García, C. J.; Soriano-Portillo, A.; Constant, S.; Frantz, R.; Lacour, J. *Inorg. Chim. Acta* **2007**, *360*, 955−960. (b) Riobé, F.; Piron, F.; Réthoré, C.; Madalan, A. M.; Gómez-García, C. J.; Lacour, J.; Wallis, J. D.; Avarvari, N. *New J. Chem.* **2011**, *35*, 2279−2286.

(14) Benmansour, S.; Coronado, E.; Giménez-Saiz, C.; Gómez-García, C. J.; Röβer, C. *Eur. J. Inorg. Chem.* **2014**, DOI: 10.1002/ejic.201402023.

(15) Whangbo, M.-H.; Williams, J. M.; Leung, P. C. W.; Beno, M. A.; Emge, T. J.; Wang, H. H. *Inorg. Chem.* **1985**, *24*, 3500−3502.

(16) Mori, H.; Tanaka, S.; Oshima, G.; Saito, G.; Mori, T.; Maruyama, Y.; Inokuchi, H. *Bull. Chem. Soc. Jpn.* **1990**, *63*, 2183−2190.

(17) Boca, R. *Coord. Chem. Rev.* **2004**, *248*, 757−902.

(18) (a) Avarvari, N.; Wallis, J. D. *J. Mater. Chem.* **2009**, *19*, 4061−4076. (b) Galán-Mascarós, J. R.; Coronado, E.; Goddard, P. A.; Singleton, J.; Coldea, A. I.; Wallis, J. D.; Coles, S. J.; Alberola, A. *J. Am. Chem. Soc.* **2010**, *132*, 9271−9273. (c) Pop, F.; Auban-Senzier, P.; Frąckowiak, A.; Ptaszyński, K.; Olejniczak, I.; Wallis, J. D.; Canadell, E.; Avarvari, N. *J. Am. Chem. Soc.* **2013**, *135*, 17176−17186. (d) Pop, F.; Laroussi, S.; Cauchy, T.; Gómez-García, C. J.; Wallis, J. D.; Avarvari, N. *Chirality* **2013**, *25*, 466−474. (e) Yang, S.; Pop, F.; Melan, C.; Brooks, A. C.; Martin, L.; Horton, P.; Auban-Senzier, P.; Rikken, G. L. J. A.; Avarvari, N.; Wallis, J. D. *CrystEngComm* **2014**, *16*, 3906−3916. (f) Pop, F.; Allain, M.; Auban-Senzier, P.; Martínez-Lillo, J.; Lloret, F.; Julve, M.; Canadell, E.; Avarvari, N. *Eur. J. Inorg. Chem.* **2014**, DOI: 10.1002/ejic.201400125. (g) Pop, F.; Auban-Senzier, P.; Canadell, E.; Rikken, G. L. J. A.; Avarvari, N. *Nat. Commun.* **2014**, *5*, 3757 DOI: 10.1038/ncomms4757.

(19) (a) Emge, T. J.; Wang, H. H.; Beno, M. A.; Williams, J. M.; Whangbo, M. H.; Evain, M. *J. Am. Chem. Soc.* **1986**, *108*, 8215−8223. (b) Stephens, D. A.; Rehan, A. E.; Compton, S. J.; Barkhau, R. A.; Williams, J. M. *Inorg. Synth.* **1986**, *24*, 130−143. (c) Batail, P.; Boubekeur, K.; Fourmigué, M.; Gabriel, J.-C. P. *Chem. Mater.* **1998**, *10*, 3005−3015.

(20) Sheldrick, G. M. *Programs for the Refinement of Crystal Structures;* University of Göttingen: Göttingen, Germany, 1996.

(21) Farrugia, L. J. *J. Appl. Crystallogr.* **1999**, *32*, 837−838.

(22) Whangbo, M.-H.; Hoffmann, R. *J. Am. Chem. Soc.* **1978**, *100*, 6093−6098.

(23) Ammeter, J. H.; Bürgi, H.-B.; Thibeault, J.; Hoffmann, R. *J. Am. Chem. Soc.* **1978**, *100*, 3686−3692.

(24) Pénicaud, A.; Boubekeur, K.; Batail, P.; Canadell, E.; Auban-Senzier, P.; Jérome, D. *J. Am. Chem. Soc.* **1993**, *115*, 4101−4112.

(25) Bain, G. A.; Berry, J. F. *J. Chem. Educ.* **2008**, *85*, 532−536.